ORIGINAL ARTICLES

UDC: 616.831-006-08
DOI: https://doi.org/10.2298/VSP250525083L

Multiparametric structural imaging biomarkers of early white matter microstructural changes during and after glioblastoma chemoradiotherapy: diffusion tensor imaging and diffusion kurtosis imaging

Multiparametrijski strukturni slikovni biomarkeri ranih promena mikrostrukture bele mase tokom i nakon hemioradioterapije glioblastoma: difuziono tenzorsko snimanje i difuziono snimanje kurtoze

Miloš Lučić*†, Igor Djan‡, Olivera Šveljo†§, Silvija Lučić*‖, Olivera Ivanov*‡, Mladen Bjelan*, Dušan Ilić§

University of Novi Sad, *Faculty of Medicine, §Faculty for Technical Sciences, Novi Sad, Serbia; Oncology Institute of Vojvodina, ‡Radiotherapy Clinic, †Radiology Department, ‖Nuclear Medicine Department, Sremska Kamenica, Serbia

Abstract

Background/Aim. Recognizing early irradiation-induced changes in the white matter is of great importance. The aim of this study was to investigate the potential use of diffusion tensor imaging (DTI) and diffusion kurtosis imaging (DKI) parameters as biomarkers of early brain tissue microstructural changes during chemoradiotherapy (CRT) treatment of newly diagnosed glioblastoma. **Methods.** A total of 42 glioblastoma patients who underwent CRT after surgical resection/biopsy were scanned three times using magnetic resonance imaging (MRI): before treatment, after 16 fractions, and after 33 fractions. Regions of interest (ROI) with total irradiation doses of 59.4 Gy (ROI 1), 39.6 Gy (ROI 2), and 19.8 Gy (ROI 3) were identified using co-registered axial dose distribution plans/dose-volume histograms and MRI scans. For each ROI, the following DTI parameters were calculated, measured, and analyzed: fractional anisotropy (FA), radial diffusivity (RD), axial diffusivity (AD), and mean diffusivity (MD). The corresponding DKI parameters included: radial kurtosis (RK), axial kurtosis (AK), and mean kurtosis (MK). **Results.** A significant decrease in FA value was observed in ROI 1 (total delivered dose 59.4 Gy) after both 16 and 33 delivered fractions, while the other DTI parameters and MK showed a significant increase. In ROI 1, a decreasing trend in RK and AK was identified, which was statistically confirmed after both 16 and 33 delivered fractions. In ROI 2 (total delivered dose of 39.6 Gy), FA values were significantly reduced after both 16 and 33 fractions, whereas RD, AD, MD, and MK were increased after 16 fractions, followed by a decrease after 33 fractions. The RK value in ROI 2 showed a significant decrease after both 16 and 33 fractions, and no changes were observed in AK values. In ROI 3 (total delivered dose of 19.8 Gy), no significant changes in any of the measured DTI or DKI parameters were noticed. **Conclusion.** DTI and DKI metric parameters may serve as biomarkers of early changes during and after CRT, providing information that may offer a better understanding of the complex dynamics of early white matter microstructural changes in response to glioblastoma CRT.

Keywords:
biomarkers; brain injuries; chemoradiotherapy; diffusion magnetic resonance imaging; diffusion tensor imaging; glioblastoma.

Apstrakt

Uvod/Cilj. Prepoznavanje ranih promena izazvanih zračenjem u beloj masi je od velike važnosti. Cilj rada bio je da se ispita mogućnost primene parametara difuzionog tenzorskog snimanja (*diffusion tensor imaging* - DTI) i difuzionog snimanja kurtoze (*diffusion kurtosis imaging* - DKI) kao biomarkera ranih promena mikrostrukture moždanog tkiva, tokom lečenja novodijagnostikovanog glioblastoma hemioradioterapijom (HRT). **Metode.** Ukupno 42 bolesnika obolela od glioblastoma, koji su posle hirurške resekcije/biopsije podvrgnuti HRT, snimljena su tri puta magnetnom rezonancom (MR): pre terapije, posle 16 frakcija i posle 33 frakcije. Regioni od interesa (ROI), sa ukupnim

Correspondence to: Miloš Lučić, University of Novi Sad, Faculty of Medicine, Hajduk Veljkova 3, 21 000 Novi Sad, Serbia.
E-mail: milos.lucic@mf.uns.ac.rs

dozama zračenja od 59,4 Gy (ROI 1), 39,6 Gy (ROI 2) i 19,8 Gy (ROI 3), identifikovani su korišćenjem koregistrovanih aksijalnih planova raspodele doze/histograma zapremine doze i snimaka MR. Za svaki ROI izračunati su, izmereni i analizirani sledeći DTI parametri: frakciona anizotropija (FA), radijalna difuzivnost (RD), aksijalna difuzivnost (AD) i srednja difuzivnost (SD). Odgovarajući DKI parametri uključivali su: radijalnu kurtozu (RK), aksijalnu kurtozu (AK) i srednju kurtozu (SK). **Rezultati.** Značajno smanjenje vrednosti FA utvrđeno je u ROI 1 (ukupna isporučena doza 59,4 Gy) posle isporučenih 16 i 33 frakcija, dok su ostali parametri DTI i SK pokazali značajno povećanje. U ROI 1 utvrđen je opadajući trend RK i AK, koji je potvrđen statistički i posle 16 i posle 33 isporučene frakcije. U ROI 2 (ukupna isporučena doza 39,6 Gy), vrednost FA bila je značajno smanjena i posle 16 i posle 33 frakcije, dok su RD, AD, SD i SK bili povećani posle 16 frakcija, a potom smanjeni posle 33 frakcije. Vrednost RK u ROI 2 pokazala je značajno smanjenje nakon 16 i 33 frakcije, a u vrednostima AK nisu ustanovljene promene. U ROI 3 (ukupna isporučena doza 19,8 Gy) nisu primećene značajne promene ni u jednom od izmerenih DTI ili DKI parametara. **Zaključak.** Metrički parametri DTI i DKI mogu poslužiti kao biomarkeri ranih promena tokom i posle HRT, obezbeđujući informacije koje pružaju bolje razumevanje složene dinamike ranih promena mikrostrukture bele mase, kao odgovor na HRT glioblastoma.

Ključne reči:
biomarkeri; mozak, povrede; radiohemioterapija; magnetna rezonanca, difuziona; snimanje, difuziono, tenzorsko; glioblastom.

Introduction

Treatment of newly diagnosed glioblastoma (GB), as one of the biologically most aggressive brain tumors in adult patients without chemoradiotherapy (CRT), is nowadays impossible to imagine [1–4]. It is believed that transient demyelination, axon impairment, and neuroinflammation are important markers of white matter injury during CRT in GB patients [5, 6]. Since these processes are vital for normal neurological functioning, treatment-induced alterations eventually lead to perivascular, diffuse demyelination and axon degeneration in later stages [6-8].

Recognizing early irradiation-induced changes in normal-appearing white matter is therefore of great importance. Although several other imaging modalities have recently been proposed, structural imaging based on diffusion-weighted magnetic resonance imaging (MRI) remains an important tool for assessing brain microstructural alterations during and after CRT treatment [9, 10]. Imaging of the brain's functional architecture became possible with the introduction of diffusion tensor imaging (DTI), a technique derived from diffusion-weighted imaging (DWI) that basically provides information on the Brownian motion of water molecules within brain tissue. The DTI technique provides insight into white matter tracts and brain tissue microstructural changes [11, 12] that could be detected even before the appearance of morphological changes, usually evaluated by conventional MRI techniques. Measurable DTI parameters such as fractional anisotropy (FA), radial diffusivity (RD), axial diffusivity (AD), and mean diffusivity (MD) are widely accepted for white matter microstructure assessment [13].

Differences in FA values, which provide information on white matter density and integrity, are observed not only between normal-appearing white matter and tumorous tissue but also between normal-appearing white matter and impaired white matter tissue during and after radiotherapy (RTh) treatment [14, 15]. RD represents diffusion magnitude perpendicular to the white matter fibers, and is associated with myelination changes, while AD represents diffusion magnitude parallel to the white matter fibers, and, as suggested by histologically correlated data, could be linked to the axonal injury [13, 16, 17]. MD is usually considered an inverse measure of membrane density, and is related to cellularity, edema, and necrosis [13, 17–19].

Besides DTI metrics, quantified with a diffusion tensor using a Gaussian distribution function, a whole new set of parameters that takes into account the non-Gaussian behavior of water molecular diffusion by mathematical calculation of the kurtosis of the diffusion displacement probability distribution, diffusion kurtosis imaging (DKI) has been translated from experimental to clinical settings [20, 21]. The degree of non-Gaussian water diffusion in kurtosis imaging is quantified using radial kurtosis (RK), axial kurtosis (AK), and mean kurtosis (MK). Some authors suggested that kurtosis metrics may complement standard diffusion metrics, and that DKI may be more sensitive to some aspects of brain tissue microstructure alterations [20, 22–24].

Several studies have shown that DKI values contribute to better discrimination between high-grade and low-grade gliomas than the conventional diffusion parameters [25–27]. DKI also appears to be a promising method for the early detection of healthy brain tissue damage during and/or after RTh treatment, potentially providing more information about mechanisms of white matter injury subsequent to brain irradiation [19]. Since both concomitant and adjuvant CRT with temozolomide have become an unavoidable part of the treatment of GB patients [1, 28, 29], and improve survival after resection or biopsy, the impact of irradiation on the healthy brain tissue, including the surrounding normal-appearing white matter, is inevitable [18, 30]. In recent years, numerous studies have been investigating chronic brain tissue and white matter injuries after the RTh treatment [30–34], among them several have used the advanced DWI MRI techniques in an attempt to identify early CRT-induced brain tissue injury [35–38].

The exact underlying pathophysiological mechanisms that result in the white matter irradiation changes are still not fully understood [35, 38–40]. Moreover, the impact of RTh doses and daily fractions on the changes that may be detectable by DTI or DKI parameters is still not discerned nor precisely determined [41, 42].

The aim of this prospective observational study was to examine the changes of DTI and DKI parameters within the white matter at three time points—before, during, and after the application of different daily and total radiation doses, as well as to evaluate whether the DTI and DKI parameters can be used as biomarkers of early white matter radiation damage during and immediately after CRT treatment in patients with GB.

Methods

Patients and treatment

The study included 42 patients with newly diagnosed GB who underwent concurrent CRT after neurosurgical resection/biopsy (25 males, 17 females; age range 31–72 years; mean age 57.28 ± 9.87). All patients were treated with fractionated focal irradiation, delivered in 33 fractions at 1.8 Gy *per* fraction, resulting in a total dose of 59.4 Gy to the gross tumor volume (GTV) with a 2–3 cm margin around the clinical target volume (CTV). Conformal RTh was delivered with linear accelerators with a nominal energy of 6 megavolts, and quality assurance was performed by means of individual case reviews. Concomitant chemotherapy, consisting of temozolomide at a dose of 75 mg/m^2/day, was applied from the beginning until the last day of RTh treatment (optimally for 42 days, but in real-life clinical settings, never longer than 49 days) [1, 43].

This study was approved by the Ethics Committee of the Oncology Institute of Vojvodina, Serbia (No. 4/18/1-972/2-8, from April 12, 2018). Written informed consent was obtained from all participants.

Delineation of target volumes

For delineation of the target volume, co-registration of axial dose distribution plans and dose volume histograms to the contrast enhanced T1-weighted (T1-w) and/or fluid-attenuated inversion recovery (FLAIR) MRI sequences were used in addition to the dedicated computerized tomography scans, that were used in the process of three-dimensional RTh planning (XiO 4.62 and Monaco 5.11, Elekta, Stockholm, Sweden).

The current European Society for Radiotherapy and Oncology (ESTRO)–Advisory Committee on Radiation Oncology Practice/European Organization for Research and Treatment of Cancer standards were used to delineate GTV, with CTV and planning target volume [44, 45]. Recently published ESTRO–European Society of Neuro-Oncology guidelines suggested a reduction of GTV to CTV margins of 0.5–1.5 cm, recommending the exclusion of subventricular zones, and margins reduced at anatomical barriers [46], while delineation of critical organs at risk remained unchanged [47].

Three regions of interest (ROI) with total irradiation doses of 59.4 Gy (ROI 1), 39.6 Gy (ROI 2), and 19.8 Gy (ROI 3) were identified using axial dose distribution plans co-registered with contrast-enhanced three-dimensional T1-w and/or FLAIR images (Figure 1A–C). Calculated daily doses were approximately 1.8 Gy for the areas with a total delivered dose of 59.4 Gy, 1.2 Gy for the areas with a delivered dose of 39.6 Gy, and 0.6 Gy for areas with a delivered dose of 19.8 Gy.

Magnetic resonance imaging data acquisition

Patients were scanned using a 3T MR scanner (Magnetom TIM Trio, Siemens, Erlangen, Germany) using a 48-channel head-phased array coil, at three different time points: immediately before the beginning of CRT treatment, after delivering 16 fractions (approximately half of the treatment), and after 33 fractions (immediately at the end of CRT treatment).

Imaging protocol included sagittal high-resolution magnetization-prepared rapid acquisition with gradient-echo

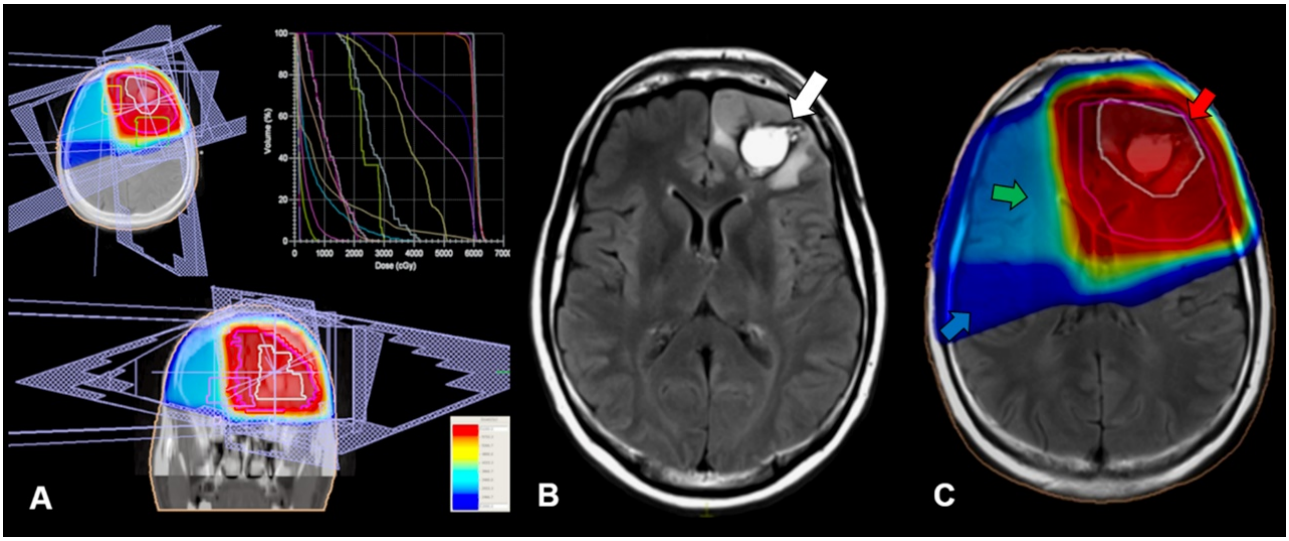

Fig. 1 – Axial dose distribution plan with dose volume histogram of a conformal radiation therapy plan for glioblastoma patient (A), superimposed to fluid-attenuated inversion recovery images, where postoperative glioblastoma is presented (white arrow) (B), and the irradiation dose distribution plan (C), with different isodose lines dividing the areas presented in different colors [red area 1.8 Gy daily/total delivered dose 59.4 Gy (red arrow); green area 1.2 Gy daily/total delivered dose 39.6 Gy (green arrow); blue area 0.6 Gy daily/total delivered dose 19.8 Gy (blue arrow)].

T1-weighted isotropic sequence before and after paramagnetic gadolinium-based contrast administration, and axial two-dimensional T2-weighted and FLAIR sequences (both 30 slices, 0.9 × 0.9 in-plane resolution, slice thickness 4 mm). For DWI acquisition, three b-values (0, 1,000, and 2,000 s/mm²) were applied along 30 diffusion-encoding directions, with 40 axial slices and an isotropic resolution of 3 mm, to calculate diffusion and kurtosis tensors. Based on these data, we measured and analyzed the following DTI parameters: FA, RD, AD, and MD. In addition, the corresponding DKI parameters—RK, AK, and MK—were also evaluated.

Only recently presented, kurtosis FA (KFA), as a potentially more accurate imaging biomarker than FA, has not been calculated or analyzed [48].

Image processing and region of data analysis

To generate FA, RD, AD, MD, RK, AK, and MK maps, the diffusional kurtosis estimator freely available software (version 2.5.1; Medical University of South Carolina, Charleston, South Carolina; https://www.nitrc.org/projects/dke/) [22] has been used.

ROI were manually selected by two radiologists with more than 10 years of experience, who assessed the maps simultaneously in a joint session, reaching a consensus on where to place the ROI 1 (total irradiation dose of 59.4 Gy), ROI 2 (total irradiation dose of 39.6 Gy), and ROI 3 (total irradiation dose of 19.8 Gy). Each ROI was of the same size, and in each of them all observed DTI parameters (FA, RD, AD, MD) and all DKI parameters (RK, AK, MK) were separately measured on the same spots in all three observed areas in three different time points: immediately before CRT treatment, after 16 delivered fractions, and after 33 delivered fractions (immediately after the end of CRT treatment) (Figure 2).

Statistical analysis

Changes in DTI and DKI parameters at different time points were analyzed using a statistical data analysis software system (StatSoft, Inc., version 12.0.1133.15; www.statsoft.com). Student's *t*-test was executed to estimate pairwise differences between average values obtained from three different imaging time-points. Average cross-subject values of measured DTI and DKI parameters were used to identify the increasing or decreasing trend of the parameters in observing time points for each ROI.

Results

Statistical differences in observed DTI and DKI parameters over time, during and after CRT treatment, compared with the initial values measured before and during treatment, are presented in Table 1.

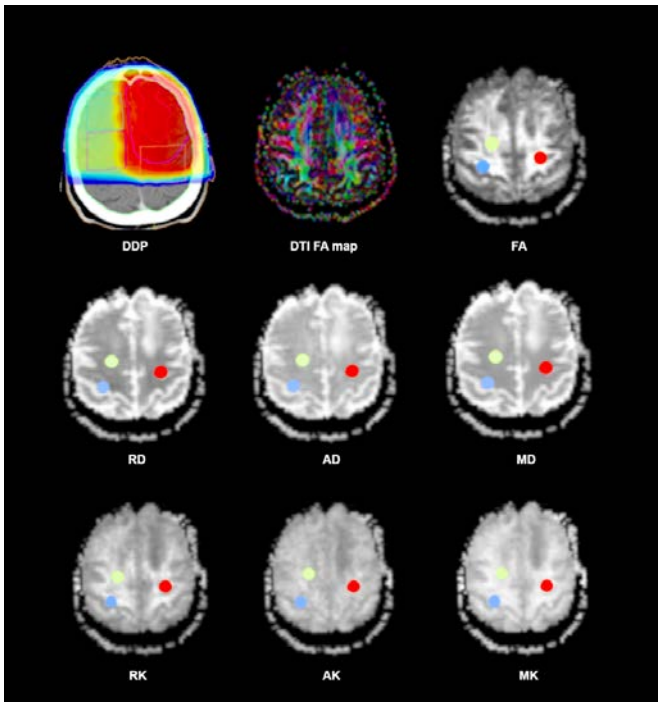

● **ROI 1** - 1.8 Gy daily fraction; overall delivered dose 59.4 Gy
● **ROI 2** - 1.2 Gy daily fraction; overall delivered dose 39.6 Gy
● **ROI 3** - 0.6 Gy daily fraction; overall delivered dose 19.8 Gy

Fig. 2 – Region of interest (ROI) identification according to co-registered radiotherapy dose distribution plan (DDP) in axial plane on different diffusion maps for measurement of diffusion tensor imaging (DTI) parameters: fractional anisotropy (FA), radial diffusivity (RD), axial diffusivity (AD), and mean diffusivity (MD), and diffusion kurtosis imaging (DKI) parameters: radial kurtosis (RK), axial kurtosis (AK), and mean kurtosis (MK) in areas with different delivered doses.

Table 1

Statistical differences of DTI and DKI parameters average values in predefined ROIs between observed time points before, during, and immediately after chemoradiotherapy

Parameter	ROI 1 (1.8 Gy/fraction)			ROI 2 (1.2 Gy/fraction)			ROI 3 (0.6 Gy/fraction)		
	16/0	33/0	33/16	16/0	33/0	33/16	16/0	33/0	33/16
DTI									
FA	0.348–0.396; < 0.05	0.304–0.396; < 0.01	0.304–0.348; < 0.05	0.324–0.368; < 0.05	0.318–0.368; < 0.05	0.318–0.324; > 0.05	0.361–0.364; > 0.05	0.359–0.364; > 0.05	0.359–0.361; > 0.05
RD	0.881–0.824; < 0.05	0.934–0.824; < 0.01	0.934–0.881; < 0.05	0.869–0.825; < 0.05	0.772–0.825; < 0.05	0.772–0.869; < 0.01	0.808–0.811; > 0.05	0.798–0.811; > 0.05	0.798–0.808; > 0.05
AD	1.489–1.376; < 0.05	1.501–1.376; < 0.05	1.501–1.489 > 0.05	1.511–1.399; < 0.05	1.288–1.399; < 0.05	1.288–1.511; < 0.01	1.387–1.377; > 0.05	1.391–1.377; > 0.05	1.391–1.387; > 0.05
MD	1.129–0.998; < 0.05	1.244–0.987; < 0.01	1.244–1.129; < 0.05	1.221–1.102; < 0.05	0.979–1.102; < 0.05	0.979–1.221; < 0.01	0.992–1.012; > 0.05	0.983–1.012; > 0.05	0.983–0.992; > 0.05
DKI									
RK	1.066–1.188; < 0.05	0.951–1.188; < 0.01	0.951–1.066; < 0.05	1.068–1.214; < 0.05	0.915–1.214; < 0.01	0.915–1.068; < 0.05	1.189–1.201; > 0.05	1.176–1.201; > 0.05	1.176–1.189; > 0.05
AK	0.675–0.799; < 0.05	0.661–0.799; < 0.05	0.601–0.675; > 0.05	0.761–0.783; > 0.05	0.774–0.783; > 0.05	0.774–0.761; > 0.05	0.776–0.791; > 0.05	0.762–0.791; > 0.05	0.762–0.776; > 0.05
MK	1.301–0.997; < 0.05	1.329–0.997; < 0.05	1.329–1.301; > 0.05	1.229–0.998; < 0.05	1.199–0.998; < 0.05	1.199–1.229; > 0.05	0.963–0.951; > 0.05	0.975–0.951; > 0.05	0.975–0.963; > 0.05

For abbreviations, see Figure 2.

All values are given as mean values. Statistical significance was set at $p < 0.05$.

Note. **16/0, 33/0, and 33/16 represent compared measurements at different time points – before, during, and after treatment: 16 vs. 0 fractions, 33 vs. 0 fractions, and 33 vs. 16 fractions.**

Within ROI 1, FA values were significantly lower in normal-appearing white matter, both after delivering 16 (1.8 Gy/fraction, total dose 28.8 Gy) and 33 fractions (1.8 Gy/fraction, total dose 59.4 Gy), compared with non-irradiated white matter before the irradiation. Average RD, AD, and MD values, as well as diffusion MK, showed a significant increase when comparing the same measurement time points within ROI 1. Regarding the DKI parameters RK and AK, a decrease in the values in the function of time was observed, and significant changes compared with pre-therapy values were noted both after 16 and 33 fractions. In ROI 1, only FA, RD, MD, and RK demonstrated a significant decrease between 16 and 33 fractions, whereas AD, AK, and MK did not show any significant changes between these time points.

In ROI 2, FA values were significantly lower after delivering 16 fractions (1.2 Gy/fraction, total dose 19.2 Gy) and 33 fractions (1.8 Gy/fraction, total dose 39.6 Gy) compared with pre-treatment values, with no significant differences between 16 and 33 fractions. Average RD, AD, and MD values increased significantly after delivering 16 fractions, but significantly decreased between 16 and 33 delivered fractions. Average RK values significantly decreased after 16 and 33 fractions within ROI 2, compared with the measured values before the CRT, while AK values remained without any significant changes. Average MK increased significantly after 16 fractions compared with pre-treatment values in ROI 2, then decreased significantly after 33 fractions. No significant changes in FA, AK, and MK values were observed between delivered 16 and 33 fractions in ROI 2.

Similar to the DTI parameters (FA, RD, AD, and MD), the DKI parameters (RK, AK, and MK) in ROI 3 did not exhibit any significant changes of the average values at the observed time points, neither after 16 delivered fractions (0.6 Gy/fraction, total dose 9.6 Gy) nor after 33 fractions (0.6 Gy/fraction, total dose 19.8 Gy), nor between the delivered 16 and 33 fractions.

Discussion

Since the initial introduction of molecular neuro-oncology into clinical practice [49], the impact of DTI metrics on the detection of brain tissue alteration of different origins, including irradiation-induced white matter injury, became the subject of research [7, 16, 17, 23, 35]. Fewer studies included non-Gaussian DKI metrics to detect early changes in brain parenchyma during CRT treatment [8, 14, 23, 50]. As the most prominent early indicators, the results of our study have demonstrated decrease of FA, and increase of MD and MK values in the normal appearing white matter, both during and immediately after CRT treatment in the brain areas with delivered dose of 28.8 Gy after 16 fractions, and total dose of 59.4 Gy after 33 fractions, and these results are coherent with the results of several other published studies [14, 19]. Both decreased FA and increased MD and MK values are considered as the consequences of demyelination, axonal loss, and/or transient cerebral edema. On the contrary, edema resolution, oligodendrocyte regeneration, and remyelination should result in increased FA and MD values [51]. As reported in the literature [19], in response to RTh, RD values typically increase, while AD values have been shown to either increase [10, 35, 42] or decrease [38, 41, 52]. In the brain areas with the delivered daily dose (DDD) of 1.8 Gy and a total dose of 59.4 Gy during and after CRT, both after delivering 16 and 33 fractions, an increase in RD values, correlating with demyelination, and AD values, which indicate axonal loss and reactive astrogliosis, was noticed [51, 53].

Unexpectedly, a decrease in RK and AK values was recorded at the same measurement time points in the same areas, even though they were expected to follow trends similar to those of RD and AD. Although the observed decreases in RK and AK values were unanticipated, they may potentially reflect transient/temporary microstructural alterations in white matter following irradiation, possibly related to processes such as edema resolution, axonal swelling, or reactive gliosis. Yet, the possibility of an unintentional computational error or another form of oversight cannot be entirely excluded. Nonetheless, the assumed explanation for the observed discrepancy between DTI- and DKI-derived parameters remains speculative and warrants validation through further investigation.

In a few published studies, we noticed a certain analogy in the discrepancy of the results perceived in the form of decreased RK and AK values in our study. Namely, opposite to the expected results of the majority of other studies, they have measured decreased MD, RD, and AD and slightly increased FA in patients after the end of CRT, though not as an early result, but in a follow-up period after 3 to 24 months [38, 41]. This, in turn, underscores the need for longer-term follow-up to clarify the sustained significance and interpretative value of both DTI and DKI metrics in GB CRT over time.

Although most conducted studies point out demyelination as the probable dominant consequence induced by RTh [19], Raschke et al. [38] concluded that neither edema nor demyelination could be a plausible reason for the decrease in diffusion. They speculated that the decreased diffusion could be the result of axonal swelling, possibly due to tissue oxygenation and vascular changes that occur after irradiation. Revealing reductions in RD and AD values after irradiation, Zhu et al. [41] proposed that RD decreases could be a sign of remyelination. In contrast, the AD decrease could be linked to astrogliosis, which may explain our results, but still does not provide a proper background for the opposite trends between RD and AD and between RK and AK in the area with a delivered total dose of 59.4 Gy, both after 16 and 33 fractions.

Still, recent investigations have revealed microstructural tissue changes not only in the hemisphere where GB is located, but also in the contralateral hemisphere, which differ even between right-sided and left-sided GB location [54]. Since this recently published feature was not considered in our study design, we strongly believe that further investigations to gain deeper insight into microstructural white matter alterations in the presence of high-grade glioma, or during and after irradiation, would be beneficial.

We found that AD, AK, and MK did not show a significant difference between 16 and 33 fractions in the area of DDD of 1.8 Gy and a total dose of 59.4 Gy. That does not

necessarily reflect a better sensitivity of MD compared to MK. The lack of statistical significance between these two time points may be explained by the higher susceptibility of MK to early irradiation-induced changes, leading to faster and more stable increases in MK values compared with MD.

In the treated brain areas with a DDD of 1.2 Gy, and a total dose of 39.6 Gy, where decrease of FA and an initial increase of RD, AD, and MD, but also MK, have been noted after 16 delivered fractions, with a later decrease of values after 33 delivered fractions. That leaves us in a belief that the initial increase and later decrease of RD, AD, MD, and MK suggest transient edema as a dominant mechanism of early white matter tissue injury, while the decrease of RK and AK both after delivering 16 and 33 fractions suggest that demyelination is included in the white matter alterations profile, rather than axonal impairment. Some authors suggest that the biological alterations are most likely occurring within the extracellular environment due to increased vascular permeability and/or reactive neuroinflammatory processes after irradiation [19, 42].

These findings are consistent with the statement that kurtosis measure is less sensitive to free fluid contamination, since the interpretability of DKI parameters depends on the accuracy of tensor estimation. Motion, noise, and/or imaging artifacts can cause significant errors, up to the level of physical/biological implausibility [15, 20–22]. That actually corresponds to our results, suggesting that DKI metrics were slightly less susceptible to radiation-induced edema detection than measured DTI parameters. Dose and time-dependent changes in irradiated white matter that have been found to correlate with several other studies' results [17, 19, 42], where measured MD, AD, RD, and MK increase and FA decrease appear earlier in areas receiving higher radiation doses. Hope et al. [35] found that MD, RD, and AD significantly increased in brain regions receiving more than 41 Gy in total dose, compared to those receiving less than 12 Gy in total, which corresponds with our results.

We found that daily doses of 0.6 Gy and total delivered dose of 19.8 Gy did not cause any significant changes in DTI or DKI metrics. This means that white matter alterations during and after CRT treatment could not be identified, neither after 16 delivered fractions, nor after 33 delivered fractions. Therefore, we may speculate that the threshold for detecting early white matter injury during or immediately after CRT treatment could actually lie somewhere above 20 Gy. Still, it should be emphasized that in several studies, changes in white matter structure for smaller delivered doses have been reported [41, 55], though not immediately, but later, in the period of 9 to 11 months after CRT [38, 42].

Although our study design includes imaging before, during, and immediately after CRT, it does not extend to post-treatment follow-up. This represents a clear limitation, as it prevents us from definitively characterizing the observed changes in DTI and DKI metrics as either transient and/or reversible effects, or as predictors of late or delayed radiation injury.

As late radiation injury was beyond the scope of the present investigation, we believe the current findings should be interpreted solely as indicative of early, and potentially transient effects of irradiation.

We would also like to emphasize that the present study did not employ repeated-measures analysis of variance or multivariate analyses, which might have provided a more robust statistical framework for assessing longitudinal changes and addressing multiple comparisons. As re-analysis is not feasible at this stage, this limitation is duly acknowledged and should be taken into consideration when interpreting the findings.

Accordingly, further comprehensive studies are warranted to fully elucidate the potential of DTI and DKI metrics as reliable biomarkers of white matter microstructural alterations during and after CRT in GB patients, in relation to time and radiation dose.

While several studies have investigated the association between neurocognitive impairment and/or clinical outcomes and both early and late radiation-induced brain injury [56–59], our study did not address this interconnection, which represents a limitation with respect to its translational relevance. Future investigations that integrate neurocognitive assessment with clinical outcomes during and after GB CRT would significantly enhance the clinical utility and applicability of DTI and DKI biomarkers in real-world neuro-oncological settings.

Recently published studies incorporating radiomics into the assessment of white matter alterations during CRT may contribute to a more profound comprehension of the sophisticated and interrelated pattern of radiation-induced brain injury [60, 61]. Furthermore, emerging and ongoing investigations focusing on cellular and molecular responses of brain tissue to specific RTh, including proton therapy, as well as the integration of artificial intelligence in the evaluation of irradiated white matter, are expected to offer novel insights into the pathophysiology of radiation-induced changes in the brain tissue [62–65].

Conclusion

Diffusion tensor imaging and diffusion kurtosis imaging metrics are susceptible to white matter alterations during and after chemoradiotherapy treatment. These metrics provide valuable insight into early irradiation-induced changes, even within normal-appearing white matter, and may prove useful as structural imaging biomarkers for identifying early, and potentially transient and/or reversible microstructural alterations related to irradiation. The application of diffusion tensor imaging and diffusion kurtosis imaging holds considerable potential to broaden our understanding of the complex dynamics underlying early microstructural alterations in white matter in response to glioblastoma chemoradiotherapy, potentially influencing future diagnostic and clinical strategies. Given that late radiation effects were not addressed within the scope of our present investigation, further longitudinal studies with extended follow-up periods would be essential to validate the potential of diffusion tensor imaging and diffusion kurtosis imaging metrics as predictors of late or delayed radiation-induced brain injury.

Acknowledgement

The authors acknowledge the financial support of the Provincial Secretariat for Science and Technology Development within the project "Multiparametric structural and metabolic imaging of the intratumorous bioarchitectonics in the function of the diagnosis and therapy improvement in patients with malignant lung and central nervous system tumours"; Grant No. 142-451-2433/2018.

R E F E R E N C E S

1. *Stupp R, Hegi ME, Gilbert MR, Chakravarti A.* Chemoradiotherapy in malignant glioma: standard of care and future directions. J Clin Oncol 2007; 25(26): 4127–36. DOI: 10.1200/JCO.2007.11.8554.
2. *Hanna C, Lawrie TA, Rogozińska E, Kernohan A, Jefferies S, Bulbeck H,* et al. Treatment of newly diagnosed glioblastoma in the elderly: a network meta-analysis. Cochrane Database Syst Rev 2020; 3(3): CD013261. DOI: 10.1002/14651858.CD013261.pub2.
3. *Qi D, Li J, Quarles CC, Fonkem E, Wu E.* Assessment and prediction of glioblastoma therapy response: challenges and opportunities. Brain 2023; 146(4): 1281–98. DOI: 10.1093/brain/awac450.
4. Obrador E, Moreno-Murciano P, Oriol-Caballo M, López-Blanch R, Pineda B, Gutiérrez-Arroyo JL, et al. Glioblastoma Therapy: Past, Present and Future. Int J Mol Sci 2024; 25(5): 2529. DOI: 10.3390/ijms25052529.
5. *De Groot JD, van Dijken BRJ, van der Weide HL, Enting RH, van der Hoorn A.* Voxel based morphometry-detected white matter volume loss after multi-modality treatment in high grade glioma patients. PLoS One 2023; 18(5): e0275077. DOI: 10.1371/journal.pone.0275077.
6. *Rafanan J, Ghani N, Kazemeini S, Nadeem-Tariq A, Shih R, Vida TA.* Modernizing Neuro-Oncology: The Impact of Imaging, Liquid Biopsies, and AI on Diagnosis and Treatment. Int J Mol Sci 2025; 26(3): 917. DOI: 10.3390/ijms26030917.
7. *Nagesh V, Tsien CI, Chenevert TL, Ross BD, Lawrence TS, Junick L,* et al. Radiation-induced changes in normal-appearing white matter in patients with cerebral tumors: a diffusion tensor imaging study. Int J Radiat Oncol Biol Phys 2008; 70(4): 1002–10. DOI: 10.1016/j.ijrobp.2007.08.020.
8. *Zakharova NE, Batalov AI, Pogosbekian EL, Chekhonin IV, Goryaynov SA, Bykanov AE,* et al. Perifocal Zone of Brain Gliomas: Application of Diffusion Kurtosis and Perfusion MRI Values for Tumor Invasion Border Determination. Cancers (Basel) 2023; 15(10): 2760. DOI: 10.3390/cancers15102760.
9. *Friedrich M, Farrher E, Caspers S, Lohmann P, Lerche C, Stoffels G,* et al. Alterations in white matter fiber density associated with structural MRI and metabolic PET lesions following multimodal therapy in glioma patients. Front Oncol 2022; 12: 998069. DOI: 10.3389/fonc.2022.998069.
10. *Lohmeier J, Radbruch H, Brenner W, Hamm B, Hansen B, Tietze A,* et al. Detection of recurrent high-grade glioma using microstructure characteristics of distinct metabolic compartments in a multimodal and integrative 18F-FET PET/fast-DKI approach. Eur Radiol 2024; 34(4): 2487–99. DOI: 10.1007/s00330-023-10141-0.
11. *Le Bihan D.* Looking into the functional architecture of the brain with diffusion MRI. Nat Rev Neurosci 2003; 4(6): 469–80. DOI: 10.1038/nrn1119.
12. *Le Bihan D, Mangin JF, Poupon C, Clark CA, Pappata S, Molko N,* et al. Diffusion tensor imaging: concepts and applications. J Magn Reson Imaging 2001; 13(4): 534–46. DOI: 10.1002/jmri.1076
13. *Le Bihan D, Iima M.* Diffusion Magnetic Resonance Imaging: What Water Tells Us about Biological Tissues. PLoS Biol 2015; 13(7): e1002203. Erratum in: PLoS Biol 2015; 13(9): e1002246. DOI: 10.1371/journal.pbio.1002246.
14. *Lin L, Bhawana R, Xue Y, Duan Q, Jiang R, Chen H,* et al. Comparative Analysis of Diffusional Kurtosis Imaging, Diffusion Tensor Imaging, and Diffusion-Weighted Imaging in Grading and Assessing Cellular Proliferation of Meningiomas. AJNR Am J Neuroradiol 2018; 39(6): 1032–8. DOI: 10.3174/ajnr.A5662.
15. *Henssen D, Meijer F, Verburg FA, Smits M.* Challenges and opportunities for advanced neuroimaging of glioblastoma. Br J Radiol 2023; 96(1141): 20211232. DOI: 10.1259/bjr.20211232.
16. *Brancato V, Nuzzo S, Tramontano L, Condorelli G, Salvatore M, Cavaliere C.* Predicting Survival in Glioblastoma Patients Using Diffusion MR Imaging Metrics-A Systematic Review. Cancers (Basel) 2020; 12(10): 2858. DOI: 10.3390/cancers12102858.
17. *Manan AA, Yahya NA, Taib NHM, Idris Z, Manan HA.* The Assessment of White Matter Integrity Alteration Pattern in Patients with Brain Tumor Utilizing Diffusion Tensor Imaging: A Systematic Review. Cancers (Basel) 2023; 15(13): 3326. DOI: 10.3390/cancers15133326.
18. *Scola E, Del Vecchio G, Busto G, Bianchi A, Desideri I, Gadda D,* et al. Conventional and Advanced Magnetic Resonance Imaging Assessment of Non-Enhancing Peritumoral Area in Brain Tumor. Cancers (Basel) 2023; 15(11): 2992. DOI: 10.3390/cancers15112992.
19. *Witzmann K, Raschke F, Troost EGC.* MR Image Changes of Normal-Appearing Brain Tissue after Radiotherapy. Cancers (Basel) 2021; 13(7): 1573. DOI: 10.3390/cancers13071573.
20. *Jensen JH, Helpern JA, Ramani A, Lu H, Kaczynski K.* Diffusional kurtosis imaging: the quantification of non-gaussian water diffusion by means of magnetic resonance imaging. Magn Reson Med 2005; 53(6): 1432–40. DOI: 10.1002/mrm.20508.
21. *Jensen JH, Helpern JA.* MRI quantification of non-Gaussian water diffusion by kurtosis analysis. NMR Biomed 2010; 23(7): 698–710. DOI: 10.1002/nbm.1518.
22. *Tabesh A, Jensen JH, Ardekani BA, Helpern JA.* Estimation of tensors and tensor-derived measures in diffusional kurtosis imaging. Magn Reson Med 2011; 65(3): 823–36. Erratum in: Magn Reson Med 2011; 65(5): 1507. DOI: 10.1002/mrm.22655
23. *Wu EX, Cheung MM.* MR diffusion kurtosis imaging for neural tissue characterization. NMR Biomed 2010; 23(7): 836–48. DOI: 10.1002/nbm.1506.
24. *Goryawala M, Mellon EA, Shim H, Maudsley AA.* Mapping early tumor response to radiotherapy using diffusion kurtosis imaging. Neuroradiol J 2023; 36(2): 198–205. DOI: 10.1177/19714009221122204.
25. *Van Cauter S, Veraart J, Sijbers J, Peeters RR, Himmelreich U, De Keyzer F,* et al. Gliomas: diffusion kurtosis MR imaging in grading. Radiology 2012; 263(2): 492–501. DOI: 10.1148/radiol.12110927.
26. *Van Cauter S, De Keyzer F, Sima DM, Sava AC, D'Arco F, Veraart J,* et al. Integrating diffusion kurtosis imaging, dynamic susceptibility-weighted contrast-enhanced MRI, and short echo time chemical shift imaging for grading gliomas. Neuro Oncol 2014; 16(7): 1010–21. DOI: 10.1093/neuonc/not304.
27. *Abdalla G, Dixon L, Sanverdi E, Machado PM, Kwong JSW, Panovska-Griffiths J,* et al. The diagnostic role of diffusional kurtosis imaging in glioma grading and differentiation of gliomas from other intra-axial brain tumours: a systematic review with

critical appraisal and meta-analysis. Neuroradiology 2020; 62(7): 791–802. DOI: 10.1007/s00234-020-02425-9.

28. *Tan AC, Ashley DM, López GY, Malinzak M, Friedman HS, Khasraw M.* Management of glioblastoma: State of the art and future directions. CA Cancer J Clin 2020; 70(4): 299–312. DOI: 10.3322/caac.21613.
29. *Wen PY, Weller M, Lee EQ, Alexander BM, Barnholtz-Sloan JS, Barthel FP,* et al. Glioblastoma in adults: a Society for Neuro-Oncology (SNO) and European Society of Neuro-Oncology (EANO) consensus review on current management and future directions. Neuro Oncol 2020; 22(8): 1073–113. DOI: 10.1093/neuonc/noaa106.
30. *Wang YX, King AD, Zhou H, Leung SF, Abrigo J, Chan YL,* et al. Evolution of radiation-induced brain injury: MR imaging-based study. Radiology 2010; 254(1): 210–8. DOI: 10.1148/radiol.09090428.
31. *Suh CH, Kim HS, Jung SC, Choi CG, Kim SJ.* Multiparametric MRI as a potential surrogate endpoint for decision-making in early treatment response following concurrent chemoradiotherapy in patients with newly diagnosed glioblastoma: a systematic review and meta-analysis. Eur Radiol 2018; 28(6): 2628–38. DOI: 10.1007/s00330-017-5262-5.
32. *Şahin S, Ertekin E, Şahin T, Özsunar Y.* Evaluation of normal-appearing white matter with perfusion and diffusion MRI in patients with treated glioblastoma. Magn Reson Mater Phy 2022; 35(1): 153–62. DOI: 10.1007/s10334-021-00990-5.
33. *Andrews RN, Dugan GO, Peiffer AM, Hawkins GA, Hanbury DB, Bourland JD,* et al. White Matter is the Predilection Site of Late-Delayed Radiation-Induced Brain Injury in Non-Human Primates. Radiat Res 2019; 191(3): 217–31. DOI: 10.1667/RR15263.1.
34. *Pan J, Qiu Z, Fu G, Liang J, Li Y, Feng Y,* et al. Non-complete recovery of temporal lobe white matter diffusion metrics at one year Post-Radiotherapy: Implications for Radiation-Induced necrosis risk. Radiother Oncol 2024; 199: 110420. DOI: 10.1016/j.radonc.2024.110420.
35. *Hope TR, Vardal J, Bjørnerud A, Larsson C, Arnesen MR, Salo RA,* et al. Serial diffusion tensor imaging for early detection of radiation-induced injuries to normal-appearing white matter in high-grade glioma patients. J Magn Reson Imaging 2015; 41(2): 414–23. DOI: 10.1002/jmri.24533.
36. *Tringale KR, Nguyen T, Bahrami N, Marshall DC, Leyden KM, Karunamuni R,* et al. Identifying early diffusion imaging biomarkers of regional white matter injury as indicators of executive function decline following brain radiotherapy: A prospective clinical trial in primary brain tumor patients. Radiother Oncol 2019; 132: 27–33. DOI: 10.1016/j.radonc.2018.11.018.
37. *Rydelius A, Bengzon J, Engelholm S, Kinhult S, Englund E, Nilsson M,* et al. Predictive value of diffusion MRI-based parametric response mapping for prognosis and treatment response in glioblastoma. Magn Reson Imaging 2023; 104: 88–96. DOI: 10.1016/j.mri.2023.09.005.
38. *Raschke F, Wesemann T, Wahl H, Appold S, Krause M, Linn J,* et al. Reduced diffusion in normal appearing white matter of glioma patients following radio(chemo)therapy. Radiother Oncol 2019; 140: 110–5. DOI: 10.1016/j.radonc.2019.06.022
39. *Witzmann K, Raschke F, Wesemann T, Löck S, Funer F, Linn J,* et al. Diffusion decrease in normal-appearing white matter structures following photon or proton irradiation indicates differences in regional radiosensitivity. Radiother Oncol 2024; 199: 110459. DOI: 10.1016/j.radonc.2024.110459.
40. *Ljusberg A, Blystad I, Lundberg P, Adolfsson E, Tisell A.* Radiation-dependent demyelination in normal appearing white matter in glioma patients, determined using quantitative magnetic resonance imaging. Phys Imaging Radiat Oncol 2023; 27: 100451. DOI: 10.1016/j.phro.2023.100451.
41. *Zhu T, Chapman CH, Tsien C, Kim M, Spratt DE, Lawrence TS,* et al. Effect of the Maximum Dose on White Matter Fiber Bundles Using Longitudinal Diffusion Tensor Imaging. Int J Radiat Oncol Biol Phys 2016; 96(3): 696–705. DOI: 10.1016/j.ijrobp.2016.07.010.
42. *Connor M, Karunamuni R, McDonald C, White N, Pettersson N, Moiseenko V,* et al. Dose-dependent white matter damage after brain radiotherapy. Radiother Oncol 2016; 121(2): 209–16. DOI: 10.1016/j.radonc.2016.10.003.
43. *Djan I, Petrović B, Erak M, Nikolić I, Lucić S.* Radiotherapy treatment planning: benefits of CT-MR image registration and fusion in tumor volume delineation. Vojnosanit Pregl 2013; 70(8): 735–9. DOI: 10.2298/vsp110404001d.
44. *Cabrera AR, Kirkpatrick JP, Fiveash JB, Shih HA, Koay EJ, Lutz S,* et al. Radiation therapy for glioblastoma: Executive summary of an American Society for Radiation Oncology Evidence-Based Clinical Practice Guideline. Pract Radiat Oncol 2016; 6(4): 217–25. DOI: 10.1016/j.prro.2016.03.007.
45. *Kruser TJ, Bosch WR, Badiyan SN, Bovi JA, Ghia AJ, Kim MM,* et al. NRG brain tumor specialists consensus guidelines for glioblastoma contouring. J Neurooncol 2019; 143(1): 157–66. DOI: 10.1007/s11060-019-03152-9.
46. *Niyazi M, Andratschke N, Bendszus M, Chalmers AJ, Erridge SC, Galldiks N,* et al. ESTRO-EANO guideline on target delineation and radiotherapy details for glioblastoma. Radiother Oncol 2023; 184: 109663. DOI: 10.1016/j.radonc.2023.109663.
47. *Mir R, Kelly SM, Xiao Y, Moore A, Clark CH, Clementel E,* et al. Organ at risk delineation for radiation therapy clinical trials: Global Harmonization Group consensus guidelines. Radiother Oncol 2020; 150: 30–9. DOI: 10.1016/j.radonc.2020.05.038.
48. *Hansen B.* An Introduction to Kurtosis Fractional Anisotropy. Am J Neuroradiol 2019; 40(10): 1638–41. DOI: 10.3174/ajnr.A6235.
49. *Weller M, Pfister SM, Wick W, Hegi ME, Reifenberger G, Stupp R.* Molecular neuro-oncology in clinical practice: a new horizon. Lancet Oncol 2013; 14(9): e370–9. Erratum in: Lancet Oncol 2015; 16(5): e199. DOI: 10.1016/S1470-2045(15)70216-0.
50. *Chakhoyan A, Woodworth DC, Harris RJ, Lai A, Nghiemphu PL, Liau LM,* et al. Mono-exponential, diffusion kurtosis and stretched exponential diffusion MR imaging response to chemoradiation in newly diagnosed glioblastoma. J Neurooncol 2018; 139(3): 651–9. DOI: 10.1007/s11060-018-2910-9.
51. *Zheng Z, Wang B, Zhao Q, Zhang Y, Wei J, Meng L,* et al. Research progress on mechanism and imaging of temporal lobe injury induced by radiotherapy for head and neck cancer. Eur Radiol 2022; 32(1): 319–30. DOI: 10.1007/s00330-021-08164-6.
52. *Voon NS, Lau FN, Zakaria R, Md Rani SA, Ismail F, Manan HA,* et al. MRI-based brain structural changes following radiotherapy of Nasopharyngeal Carcinoma: A systematic review. Cancer Radiother 2021; 25(1): 62–71. DOI: 10.1016/j.canrad.2020.07.008.
53. *Xie X, Feng M, Rong Y, Hu J, Zhou W, Li Y,* et al. Whole brain atlas-based diffusion kurtosis imaging parameters for the evaluation of multiple cognitive-related brain microstructure injuries after radiotherapy in lung cancer patients with brain metastasis. Quant Imaging Med Surg 2023; 13(8): 5321–32. DOI: 10.21037/qims-22-1376.
54. *Genç B, Aslan K, Özçağlayan A, İncesu L.* Microstructural abnormalities in the contralateral normal-appearing white matter of glioblastoma patients evaluated with advanced diffusion imaging. Magn Reson Med Sci 2024; 23(4): 479–86. DOI: 10.2463/mrms.mp.2023-0054.
55. *He L, Chen M, Li H, Shi X, Qiu Z, Xu X.* Differentiation between high-grade gliomas and solitary brain metastases based on multidiffusion MRI model quantitative analysis. Front Oncol 2024; 14: 1401748. DOI: 10.3389/fonc.2024.1401748.

56. *Rübe CE, Raid S, Palm J, Rübe C.* Radiation-Induced Brain Injury: Age Dependency of Neurocognitive Dysfunction Following Radiotherapy. Cancers (Basel) 2023; 15(11): 2999. DOI: 10.3390/cancers15112999.
57. *Zegers CML, Offermann C, Dijkstra J, Compter I, Hoebers FJP, de Ruysscher D,* et al. Clinical implementation of standardized neurocognitive assessment before and after radiation to the brain. Clin Transl Radiat Oncol 2023; 42: 100664. DOI: 10.1016/j.ctro.2023.100664.
58. *Mesny E, Jacob J, Noël G, Bernier MO, Ricard D.* Specific radiosensitivity of brain structures (areas or regions) and cognitive impairment after focal or whole brain radiotherapy: A review. Cancer Radiother 2025; 29(3): 104625. DOI: 10.1016/j.canrad.2025.104625.
59. *Zhu L, Ma Y, Kong A, Wu X, Ren Y, Zhou W,* et al. Non-invasive and sensitive MRI assessment of radiation-induced cognitive dysfunction via voxel-based morphological and functional connectivity. Acta Neuropathol Commun 2025; 13(1): 180. DOI: 10.1186/s40478-025-02092-y.
60. *Chen M, Wang L, Gong G, Yin Y, Wang P.* Quantitative study of the changes in brain white matter before and after radiotherapy by applying multi-sequence MR radiomics. BMC Med Imaging 2022; 22(1): 86. DOI: 10.1186/s12880-022-00816-3.
61. *Alshuhri MS, Al-Mubarak HF, Qaisi A, Alhulail AA, AlMansour AGM, Madkhali Y,* et al. MRI Delta Radiomics to Track Early Changes in Tumor Following Radiation: Application in Glioblastoma Mouse Model. Biomedicines 2025; 13(4): 815. DOI:10.3390/biomedicines13040815
62. *Wang Y, Tian J, Liu D, Li T, Mao Y, Zhu C.* Microglia in radiation-induced brain injury: Cellular and molecular mechanisms and therapeutic potential. CNS Neurosci Ther 2024; 30(6): e14794. DOI: 10.1111/cns.14794.
63. *Winter SF, Gardner MM, Karschnia P, Vaios EJ, Grassberger C, Bussière MR,* et al. Unique brain injury patterns after proton vs photon radiotherapy for WHO grade 2-3 gliomas. Oncologist 2024; 29(12): e1748–61. DOI: 10.1093/oncolo/oyae195.
64. *Franco D, Granata V, Fusco R, Grassi R, Nardone V, Lombardi L,* et al. Artificial intelligence and radiation effects on brain tissue in glioblastoma patient: preliminary data using a quantitative tool. Radiol Med 2023; 128(7): 813–27. DOI: 10.1007/s11547-023-01655-0.
65. *Zhao J, Vaios E, Yang Z, Lu K, Floyd S, Yang D,* et al. Radiogenomic explainable AI with neural ordinary differential equation for identifying post-SRS brain metastasis radionecrosis. Med Phys 2025; 52(4): 2661–74. DOI: 10.1002/mp.17635.

Received on May 25, 2025
Revised on September 19, 2025
Revised on October 29, 2025
Accepted on November 5, 2025
Online First December 2025